Robotica (2019) volume 37, pp. 358–377. © Cambridge University Press 2018
doi:10.1017/S0263574718001054

Design, analysis and optimization of Hex4, a new 2R1T overconstrained parallel manipulator with actuation redundancy

Lingmin Xu[†], Genliang Chen[‡], Wei Ye[†], Qinchuan Li[†,*]

[†]*Faculty of Mechanical Engineering and Automation, Zhejiang Sci-Tech University, Hangzhou 310018, China. E-mails: xulingmin1993@163.com, wye@zstu.edu.cn*
[‡]*State Key Laboratory of Mechanical System and Vibration, Shanghai Key Laboratory of Digital Manufacture for Thin-Walled Structures, Shanghai Jiao Tong University, Shanghai 200240, China. E-mail: leungchan@sjtu.edu.cn*

(Accepted September 17, 2018. First published online: October 9, 2018)

SUMMARY
PMs with two rotations and one translation (2R1T) have been used as skeletons in various advanced manufacturing equipment where high accuracy and stiffness are basic requirements. Considering the advantages of redundant actuation and overconstrained structure, such as reduced singularities and improved stiffness, a new 2R1T overconstrained PM with actuation redundancy, called Hex4, is proposed in this paper. This is a 2-PUR/2-RPU PM (where P denotes an actuated prismatic joint, U a universal joint, and R a revolute joint) that is actuated by four prismatic joints. Compared with some existing 2R1T overconstrained PMs with actuation redundancy, the main advantage of the proposed PM is that the heavy motors of two limbs are mounted on the base to reduce the movable mass and improve dynamic response. First, mobility analysis, inverse kinematics, and velocity analysis are presented. Then, the local transmission index and good transmission workspace are used to evaluate the motion/force transmissibility of the Hex4 PM. The variation tendencies of the two indices with different link parameters are investigated. The singularity is then discussed by considering the motion/force transmissibility. Finally, link parameters are optimized to obtain an improved good transmission workspace. It is shown that the proposed PM has a good potential for high precision applications.

KEYWORDS: Parallel manipulator, Actuation redundancy, Overconstrained structure, Optimal design.

1. Introduction

In recent years, parallel manipulators (PMs) have drawn considerable interest from both academia and industry.[1−7] It should be mentioned that we only consider the PMs with rigid links in this paper. Benefitting from their closed loop structures, PMs have improved accuracy, rigidity, and loading capability when compared with the serial architectures. In particularly, three degrees-of-freedom (DOFs) PMs with two rotations and one translation (2R1T) have been used as parallel modules in various manufacturing equipment where high accuracy and stiffness are required.[1−4] Z3 head,[2] Exechon,[3] and Tricept[4] are typical examples of successful application.

High accuracy and stiffness should be regarded as important criteria to evaluate whether a 2R1T PM is suitable for some advanced manufacturing applications, for example, five-axis machining. Considering the advantages of redundant actuation, such as the elimination of singularities and improved stiffness, a 2R1T PM with actuation redundancy may be a good choice to achieve high accuracy and stiffness. There are two ways to implement actuation redundancy in a PM: either replace passive joints with actuated joints, or add an actuated limb chain without changing the mobility of

* Corresponding author. E-mail: lqchuan@zstu.edu.cn

the PM.[8,9] The latter is the preferred approach because it leads to higher stiffness and better force distribution. Much progress has been made concerning kinematic analysis, force distribution, stiffness analysis, and singularities in relation to the latter category.[10−25] This work also focuses on the latter type of redundantly actuated 2R1T PMs.

Different from the PMs with proper constraint, the overconstrained PM is a special type of PM that some constraint wrenches acting on the moving platform are linearly dependent. These common or redundant constraints increase the capability to act against the external force/torque without affecting the mobility of the PM. The overconstrained systems are suitable for industrial applications requiring high rigidity and large payload.[26,27] Therefore, a 2R1T PM with an overconstrained structure can be regarded as a way to achieve high precision applications. The Exechon robot[3] used for machining, drilling, and assembling tasks is a typical example of successful application that is based on a 2UPR-SPR overconstrained PM. Here, U, P, R, and S denote the universal joint, actuated prismatic joint, revolute joint, and spherical joint, respectively.

For reasons of structural and actuation symmetry, there is a tendency to add limited DOFs limbs with actuation to a 2R1T PM to construct a redundantly actuated 2R1T PM with overconstrained structure. However, it is a very challenging task because the added limited-DOFs limb introduces new structural constraints and may change the mobility of the target PM. The well-known 2R1T PM with non-redundant actuation and proper constraint, 3-RPS PM, proposed by Hunt[1] as an example, is composed of a fixed base, a moving platform, and three identical rigid RPS limbs. The three constrained wrenches generated by three limbs restrict one rotational and two translational motions of the moving platform. Adding a limited-DOFs limb, for example, an actuated RPS limb, to the 3-RPS PM yields a 4-RPS PM with mobility that differs from that of the 3-RPS PM. The change in mobility is caused by the constraint generated by the new RPS limb, which changes the constraint system that is spanned by all limb constraints. In contrast, it is feasible to add a 6DOF SPS limb to a 3-RPS PM to implement redundant actuation without changing the mobility of the 3-RPS PM, because the added SPS limb imposes no constraints on the moving platform, namely, the 3-RPS/SPS PM is a redundantly actuated PM with proper constraint.

To the best of our knowledge, there are only several redundantly actuated 2R1T PMs with overconstrained structure, such as 2-UPR/2-RPU,[28] 2-URR/2-RRU,[28] and 2UPR-2PRU,[29] where R denotes the actuated revolute joint. A new 2R1T 2-PUR/2-RPU overconstrained PM with actuation redundancy is presented, hereinafter referred to as Hex4. The Hex4 PM belongs to the family of RPR-equivalent PM.[30] Compared with some existing 2R1T PMs with actuation redundancy and overconstrained structure, the main advantages of the proposed PM are a reduction in the movable mass and an improved dynamic response produced by the fixed linear motors of the two PUR limbs. Meanwhile, this PM has high stiffness because of its overconstrained structure.

Kinematic performance evaluation of a PM is indispensable in the pre-design stage. Based on the algebraic characteristics of the Jacobian matrix of a PM, several indices have been proposed and widely used for performance evaluation, including manipulability[31] and condition number.[32] However, there is much controversy surrounding about these Jacobian-based indices: (a) they are coordinate dependent; and (b) the units of the elements of the Jacobian matrix are inconsistent when applied to PMs with both rotational and translational DOFs.[33] These inherent characteristics lead to unclear physical meanings and subsequently cause erroneous interpretations.

To avoid the drawbacks associated with Jacobian-based indices, motion/force transmission index[34−40] based on screw theory[41] can be used to evaluate the kinematic performance. This index describes the ability of the linkages to transmit input motion/force to the output link, or the ability to sustain the payload applied to the end effector. A local minimized transmission index (LMTI)[39,40] for transmission evaluation of redundantly actuated PMs has been proposed that separated the redundantly actuated PM into a set of non-redundant PMs by removing the redundant limbs from the redundantly actuated PM in turn. Despite the coordinate independence of this index, the influences of the redundant actuator and limb are not considered. Here, we use a new index proposed by the authors[28] for the performance evaluation and dimensional optimization of Hex4. First, by locking some actuators in an ergodic manner, the targeted redundantly actuated PM is separated into several subsidiary one-DOF PMs that are actuated by two or more actuators. Then, the index of output transmission performance is proposed by calculating the mean value of the instantaneous power produced by these one-DOF PMs. Finally, a local transmission index (LTI) is defined as the minimum value of the index of output and

https://doi.org/10.1017/S0263574718001054 Published online by Cambridge University Press

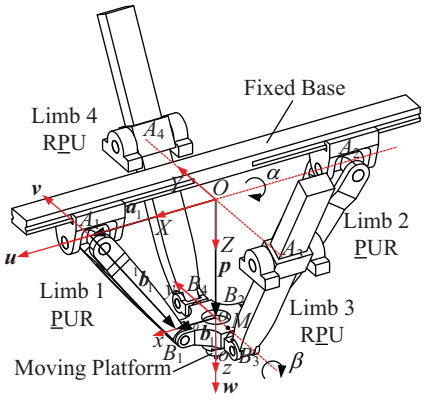

(a)

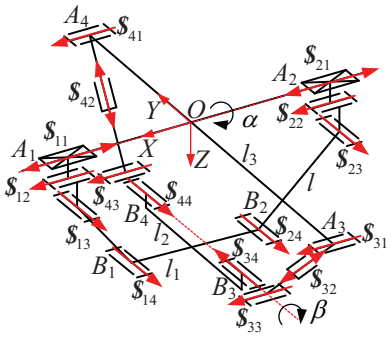

(b)

Fig. 1. Hex4 parallel manipulator: (a) CAD model and (b) schematic representation.

input transmission performance. The LTI is coordinate free and dimensionless. Compared to other indices, this index considers the influences of redundant actuator and limb, and describes the intrinsic characteristic of a redundantly actuated PM more precisely. In this paper, this index is also used to analyze the singularities of the Hex4 PM.

This paper is organized as follows. Section 2 describes the Hex4 PM. Section 3 presents the mobility analysis using Lie group theory. Sections 4 and 5 deal with the inverse kinematics and velocity, respectively. Section 6 presents the motion/force transmission performance atlases of the LTI and the good transmission workspace (GTW). Section 7 discusses the singularities of the PM in detail. Section 8 illustrates the optimization procedure considering the GTW. Section 9 presents the conclusions.

2. Description of the HEX4 Parallel Manipulator

A computer-aided design (CAD) model and a schematic of the Hex4 PM are shown in Fig. 1. The moving platform is connected to a fixed base by four actuated kinematic limbs. The first limb A_1B_1 and second limb A_2B_2 are two identical PUR kinematic chains in which the first revolute axes of the U joints are coincident with each other. The second revolute axes of the U joints are parallel to the axis of the R joint connected to the moving platform and are perpendicular to the P joints. The third limb A_3B_3 and fourth limb A_4B_4 are RPU kinematic chains. The axes of the R joints in limbs 3 and 4 are perpendicular to the P joints and parallel to the first revolute axes of the U joints in limbs 3 and 4. Meanwhile, the second revolute axes connected to the moving platform are coincident with each other. The position and orientations of the moving platform can be determined by combining the four displacements of the actuated P joints.

Let A_1 and A_2 denote the centers of the U joints in limbs 1 and 2, respectively, and let A_3 and A_4 denote the centers of the R joints in limbs 3 and 4, respectively. The centers of the R joints in limbs

https://doi.org/10.1017/S0263574718001054 Published online by Cambridge University Press

Table I. Kinematic joints and Lie subgroups of displacements.

Lie subgroups	Motion	Associated kinematic joints
$\{\boldsymbol{R}(N, \boldsymbol{u})\}$	Rotation around the axis in direction $\boldsymbol{u}$ and passing through point N	Revolute joint
$\{\boldsymbol{T}(\boldsymbol{s})\}$	Translation along vector $\boldsymbol{s}$	Prismatic joint
$\{\mathbf{C}(N,\mathbf{u})\}$	Cylindrical motion of a given axis $(N, \boldsymbol{u})$	Cylindrical joint
$\{\mathbf{G}(\mathbf{u})\}$	Gliding motion (two translations and a rotation) in a plane perpendicular to vector $\boldsymbol{u}$	Planar joint

1 and 2 are denoted by B_1 and B_2, respectively, while the centers of the U joints in limbs 3 and 4 are denoted by B_3 and B_4, respectively.

Coordinate frames are established as shown in Fig. 1(a). A fixed coordinate frame *O-XYZ* is attached to the fixed base. The origin O is at the midpoint of A_3A_4. We let the X-axis always point in the direction of OA_1, the Y-axis point along OA_4, and the Z axis point vertically downward. A moving coordinate frame *o-xyz* is attached to the moving platform (Fig. 1(a)) with its x-axis along oB_1 and its y-axis along oB_4. The z-axis points vertically downward with respect to the mobile platform. The lengths of the linkages in the Hex4 PM are defined as follows: $A_1B_1 = A_2B_2 = l$, $oo' = H$, $oB_1 = oB_2 = l_1$, $oB_3 = oB_4 = l_2$, and $OA_3 = OA_4 = l_3$.

3. Mobility Analysis

Analysis of the mobility of the Hex4 mechanism is conducted here using Lie group theory.[42] To assist the reader, we give a brief introduction to this theory. The sets of relative motion (also called motion sets) allowed by the revolute, prismatic, cylindrical, and planar joints are displacement Lie subgroups, as listed in Table I.

The motion set of the moving platform in a parallel mechanism is given by the intersection of kinematic bonds associated with all the limbs connected to that platform, i.e.

$$\{M\} = \bigcap_{i=1}^{n} \{L_i\}, \tag{1}$$

where $\{M\}$ denotes the motion set of the moving platform, $\{L_i\}$ is the kinematic bond of limb i, $\cap$ is the intersection sign in Lie group theory, and n is the number of limbs. In the Hex4 PM, the kinematic bond of limb 1 is given as

$$\{L_1\} = \{\boldsymbol{T}(\boldsymbol{u})\}\{\boldsymbol{R}(A_1, \boldsymbol{u})\}\{\boldsymbol{R}(A_1, \boldsymbol{v})\}\{\boldsymbol{R}(B_1, \boldsymbol{v})\}, \tag{2}$$

where $\boldsymbol{u}$ and $\boldsymbol{v}$ are the directional vectors of the first and second rotational axes, respectively, of the universal joint. It is easy to show that the first two subgroups $\{\boldsymbol{T}(\boldsymbol{u})\}\{\boldsymbol{R}(A_1, \boldsymbol{u})\}$ constitute a cylindrical subgroup$\{\boldsymbol{C}(A_1, \boldsymbol{u})\}$. Because of the closure of products in $\{\boldsymbol{C}(A_1, \boldsymbol{u})\}$, we have

$$\{L_1\} = \{\boldsymbol{R}(A_1, \boldsymbol{u})\}\{\boldsymbol{T}(\boldsymbol{u})\}\{\boldsymbol{R}(A_1, \boldsymbol{v})\}\{\boldsymbol{R}(B_1, \boldsymbol{v})\}. \tag{3}$$

Because vector $\boldsymbol{u}$ remains perpendicular to vector $\boldsymbol{v}$, the combination of the last three subgroups in Eq. (3) can be regarded as the kinematic bond of a planar subgroup $\{\boldsymbol{G}(\boldsymbol{v})\}$. Hence, Eq. (3) can be written as

$$\{L_1\} = \{\boldsymbol{R}(A_1, \boldsymbol{u})\}\{\boldsymbol{G}(\boldsymbol{v})\}. \tag{4}$$

Similarly, the kinematic bond of limb 2 can be identified as

$$\{L_2\} = \{\boldsymbol{R}(A_2, \boldsymbol{u})\}\{\boldsymbol{G}(\boldsymbol{v})\}. \tag{5}$$

https://doi.org/10.1017/S0263574718001054 Published online by Cambridge University Press

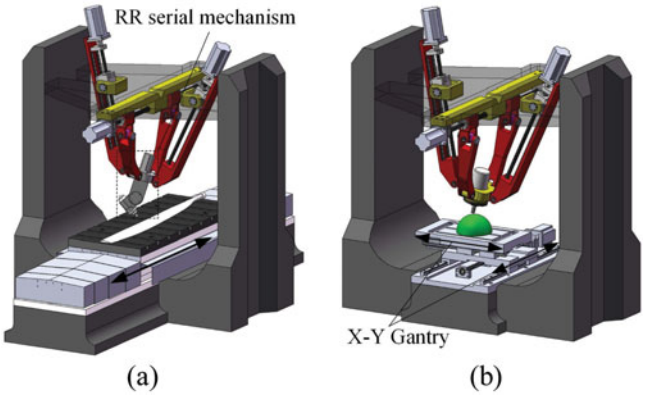

Fig. 2. Possible applications of a Hex4 PM: (a) large-scale workpiece machining and (b) five-face milling machining.

The first rotational axes of the universal joints in limbs 1 and 2 are coincident and parallel to vector $\boldsymbol{u}$, which means $\{\boldsymbol{R}(A_1, \boldsymbol{u})\} = \{\boldsymbol{R}(A_2, \boldsymbol{u})\} = \{\boldsymbol{R}(O, \boldsymbol{u})\}$.

So we have

$$\begin{aligned} \{L_1\} \cap \{L_2\} &= \{\boldsymbol{R}(A_1, \boldsymbol{u})\}\{\boldsymbol{G}(\boldsymbol{v})\} \cap \{\boldsymbol{R}(A_2, \boldsymbol{u})\}\{\boldsymbol{G}(\boldsymbol{v})\} \\ &= \{\boldsymbol{R}(O, \boldsymbol{u})\}\{\boldsymbol{G}(\boldsymbol{v})\}. \end{aligned} \tag{6}$$

The kinematic bond of limb 3 is

$$\{L_3\} = \{\boldsymbol{R}(A_3, \boldsymbol{u})\}\{\boldsymbol{T}(\boldsymbol{x})\}\{\boldsymbol{R}(B_3, \boldsymbol{u})\}\{\boldsymbol{R}(B_3, \boldsymbol{v})\}, \tag{7}$$

where vector $\boldsymbol{x}$ is along the axis of the prismatic joint. Since $\boldsymbol{x}$ is perpendicular to $\boldsymbol{u}$, the first three subgroups in Eq. (7) constitute a planar subgroup. Hence, we have

$$\{L_3\} = \{\boldsymbol{G}(\boldsymbol{u})\}\{\boldsymbol{R}(B_3, \boldsymbol{v})\}. \tag{8}$$

Similarly, the kinematic bond of limb 4 is identified as

$$\{L_4\} = \{\boldsymbol{G}(\boldsymbol{u})\}\{\boldsymbol{R}(B_4, \boldsymbol{v})\}. \tag{9}$$

In limbs 3 and 4, the second rotational axes of the universal joints are coincident and parallel to vector $\boldsymbol{v}$, which means $\{\boldsymbol{R}(B_3, \boldsymbol{v})\} = \{\boldsymbol{R}(B_4, \boldsymbol{v})\} = \{\boldsymbol{R}(M, \boldsymbol{v})\}$ (M is an arbitrary point on line B_3B_4).

So we have

$$\begin{aligned} \{L_3\} \cap \{L_4\} &= \{\boldsymbol{G}(\boldsymbol{u})\}\{\boldsymbol{R}(B_3, \boldsymbol{v})\} \cap \{\boldsymbol{G}(\boldsymbol{u})\}\{\boldsymbol{R}(B_4, \boldsymbol{v})\} \\ &= \{\boldsymbol{G}(\boldsymbol{u})\}\{\boldsymbol{R}(M, \boldsymbol{v})\}. \end{aligned} \tag{10}$$

Therefore, the motion set of the moving platform is

$$\begin{aligned} \{M\} &= \{L_1\} \cap \{L_2\} \cap \{L_3\} \cap \{L_4\} \\ &= \{\boldsymbol{R}(O, \boldsymbol{u})\}\{\boldsymbol{G}(\boldsymbol{v})\} \cap \{\boldsymbol{G}(\boldsymbol{u})\}\{\boldsymbol{R}(M, \boldsymbol{v})\} \\ &= \{\boldsymbol{R}(O, \boldsymbol{u})\}\{\boldsymbol{T}(\boldsymbol{w})\}\{\boldsymbol{R}(M, \boldsymbol{v})\}, \end{aligned} \tag{11}$$

in which $\boldsymbol{w}$ is a vector that is perpendicular to both $\boldsymbol{u}$ and $\boldsymbol{v}$. Equation (11) means that the Hex4 PM has two rotations and one translation, with one rotation around line A_1A_2 and the other around line B_3B_4. The mechanism is a typical RPR-type parallel mechanism.[5,28] In terms of its applications, the proposed PM could be used in machining a workpiece with a curved surface by adding an articulated RR serial chain (Fig. 2(a)) or mounting it on an X–Y gantry (Fig. 2(b)).

https://doi.org/10.1017/S0263574718001054 Published online by Cambridge University Press

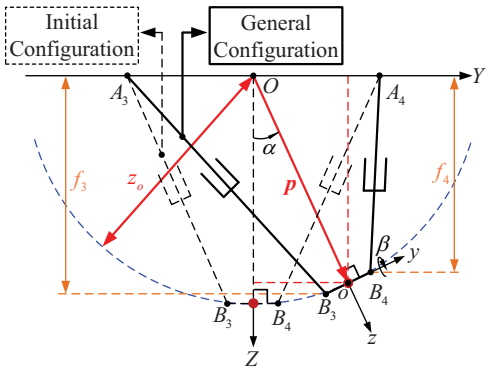

Fig. 3. Relationship between the rotational angle α and the position vector $\boldsymbol{p}$.

4. Inverse Kinematics

Determining the inverse kinematics of the Hex4 PM involves determining the actuated displacements (q_1, q_2, q_3, q_4) given the orientations and position (α, β, z_o) of the moving platform, where q_i $(i = 1, 2, 3, 4)$ denotes the distance between the point O and A_i when $i = 1, 2$, and the distance between the point A_i and B_i when $i = 3, 4$. α and β denote the rotational angel around the X-axis and y-axis, respectively, and z_o denotes the operation distance between the point O and o. Here, the values of rotational angles α and β are assumed to be zero when the moving platform is parallel to the fixed base.

The rotation matrix between the o-xyz and the O-XYZ can be written as

$$\begin{aligned} {}^{O}\boldsymbol{R}_o &= \boldsymbol{R}_X(\alpha)\boldsymbol{R}_y(\beta) \\ &= \begin{pmatrix} 1 & 0 & 0 \\ 0 & \mathrm{c}_\alpha & \mathrm{s}_\alpha \\ 0 & -\mathrm{s}_\alpha & \mathrm{c}_\alpha \end{pmatrix} \begin{pmatrix} \mathrm{c}_\beta & 0 & \mathrm{s}_\beta \\ 0 & 1 & 0 \\ -\mathrm{s}_\beta & 0 & \mathrm{c}_\beta \end{pmatrix}, \\ &= \begin{pmatrix} \mathrm{c}_\beta & 0 & \mathrm{s}_\beta \\ -\mathrm{s}_\alpha \mathrm{s}_\beta & \mathrm{c}_\alpha & \mathrm{s}_\alpha \mathrm{c}_\beta \\ -\mathrm{c}_\alpha \mathrm{s}_\beta & -\mathrm{s}_\alpha & \mathrm{c}_\alpha \mathrm{c}_\beta \end{pmatrix} \end{aligned} \tag{12}$$

where $\boldsymbol{R}_X(\alpha)$ and $\boldsymbol{R}_y(\beta)$ represent the rotational matrices around X-axis and y-axis, respectively. The s and c denote the sine and cosine functions, respectively.

As shown in Fig. 1, the position vector $\boldsymbol{A_iB_i}$ with respect to O-XYZ is denoted by ${}^{i}\boldsymbol{b}_i$ $(i = 1, 2, 3, 4)$. Because of the structural constraints, the point o is always limited into the plane YOZ, and the coordinates of the point o with respect to the O-XYZ can be defined as $\boldsymbol{p} = (0\ z_o\mathrm{s}_\alpha\ z_o\mathrm{c}_\alpha)^{\mathrm{T}}$, as shown in Fig. 3. The position vectors $\boldsymbol{OA}_i$ and $\boldsymbol{oB}_i$ with respect to the fixed frame are denoted by $\boldsymbol{a}_i$ and ${}^{o}\boldsymbol{b}_i$, respectively, and can be written as

$$\begin{cases} \boldsymbol{a}_1 = \begin{pmatrix} q_1 & 0 & 0 \end{pmatrix}^{\mathrm{T}} \\ \boldsymbol{a}_2 = \begin{pmatrix} -q_2 & 0 & 0 \end{pmatrix}^{\mathrm{T}} \\ \boldsymbol{a}_3 = \begin{pmatrix} 0 & -l_3 & 0 \end{pmatrix}^{\mathrm{T}} \\ \boldsymbol{a}_4 = \begin{pmatrix} 0 & l_3 & 0 \end{pmatrix}^{\mathrm{T}} \end{cases}, \tag{13a}$$

and

$$\begin{cases} {}^{o}\boldsymbol{b}_1 = {}^{O}\boldsymbol{R}_o \begin{pmatrix} l_1 & 0 & 0 \end{pmatrix}^{\mathrm{T}} \\ {}^{o}\boldsymbol{b}_2 = {}^{O}\boldsymbol{R}_o \begin{pmatrix} -l_1 & 0 & 0 \end{pmatrix}^{\mathrm{T}} \\ {}^{o}\boldsymbol{b}_3 = {}^{O}\boldsymbol{R}_o \begin{pmatrix} 0 & -l_2 & 0 \end{pmatrix}^{\mathrm{T}} \\ {}^{o}\boldsymbol{b}_4 = {}^{O}\boldsymbol{R}_o \begin{pmatrix} 0 & l_2 & 0 \end{pmatrix}^{\mathrm{T}} \end{cases}. \tag{13b}$$

https://doi.org/10.1017/S0263574718001054 Published online by Cambridge University Press

Through geometric constraint, the position vectors ${}^{i}\boldsymbol{b}_i$ can be written in the form

$$ {}^{i}\boldsymbol{b}_i = \boldsymbol{p} + {}^{o}\boldsymbol{b}_i - \boldsymbol{a}_i. \tag{14} $$

Using Eqs. (12)–(14), the inverse kinematics of the Hex4 PM can be written as

$$ \begin{cases} q_1 = l_1 c_\beta + e_1 \\ q_2 = l_1 c_\beta + e_2 \\ q_3 = \sqrt{e_3^2 + f_3^2} \\ q_4 = \sqrt{e_4^2 + f_4^2} \end{cases}, \tag{15} $$

where $e_1 = \sqrt{l^2 - (z_o - l_1 \mathrm{s}_\beta)^2}$, $e_2 = \sqrt{l^2 - (z_o + l_1 \mathrm{s}_\beta)^2}$, $e_3 = l_3 - l_2 \mathrm{c}_\alpha + z_o \mathrm{s}_\alpha$, $e_4 = l_3 - l_2 \mathrm{c}_\alpha - z_o \mathrm{s}_\alpha$, $f_3 = z_o \mathrm{c}_\alpha + l_2 \mathrm{s}_\alpha$, and $f_4 = z_o \mathrm{c}_\alpha - l_2 \mathrm{s}_\alpha$.

5. Velocity Analysis

Here, the Jacobian matrix represents the mapping between the rates $\dot{\boldsymbol{q}} = (\dot{q}_1\ \dot{q}_2\ \dot{q}_3\ \dot{q}_4)^{\mathrm{T}}$ of the actuators and the velocity $\dot{\boldsymbol{X}} = (\dot{\alpha}\ \dot{\beta}\ \dot{z}_o)^{\mathrm{T}}$ of the moving platform. Differentiating both sides of Eq. (15) leads to

$$ \boldsymbol{J}_q \dot{\boldsymbol{q}} = \boldsymbol{J}_x \dot{\boldsymbol{X}}, \tag{16} $$

where

$$ \boldsymbol{J}_q = \begin{pmatrix} J_{q_{11}} & 0 & 0 & 0 \\ 0 & J_{q_{22}} & 0 & 0 \\ 0 & 0 & J_{q_{33}} & 0 \\ 0 & 0 & 0 & J_{q_{44}} \end{pmatrix}, \boldsymbol{J}_x = \begin{pmatrix} J_{x_{11}} & J_{x_{12}} & J_{x_{13}} \\ J_{x_{21}} & J_{x_{22}} & J_{x_{23}} \\ J_{x_{31}} & J_{x_{32}} & J_{x_{33}} \\ J_{x_{41}} & J_{x_{42}} & J_{x_{43}} \end{pmatrix}, $$

$$ J_{q_{11}} = e_1, J_{q_{22}} = e_2, J_{q_{33}} = q_3, J_{q_{44}} = q_4, J_{x_{11}} = 0, J_{x_{12}} = z_o l_1 \mathrm{c}_\beta - q_1 l_1 \mathrm{s}_\beta, J_{x_{13}} = l_1 \mathrm{s}_\beta - z_o, $$

$$ J_{x_{21}} = 0, J_{x_{22}} = -z_o l_1 \mathrm{c}_\beta - q_2 l_1 \mathrm{s}_\beta, J_{x_{23}} = -l_1 \mathrm{s}_\beta - z_o, J_{x_{31}} = l_3(l_2 \mathrm{s}_\alpha + z_o \mathrm{c}_\alpha), J_{x_{32}} = 0, $$

$$ J_{x_{33}} = z_o + l_3 s_\alpha, J_{x_{41}} = l_3(l_2 \mathrm{s}_\alpha - z_o \mathrm{c}_\alpha), J_{x_{42}} = 0, \textit{and}\ J_{x_{43}} = z_o - l_3 \mathrm{s}_\alpha. $$

Multiplying both sides of Eq. (16) with $\boldsymbol{J}_q^{-1}$ yields

$$ \dot{\boldsymbol{q}} = \boldsymbol{J}_q^{-1} \boldsymbol{J}_x \dot{\boldsymbol{X}} = \boldsymbol{J} \dot{\boldsymbol{X}}, \tag{17} $$

where $\boldsymbol{J}$ is a 4×3 Jacobian matrix.

6. Motion/Force Transmissibility

6.1. Local transmission index for redundantly actuated PMs

The LTI[38] is important for evaluating the performance of a PM. It can be divided into two parts, the input transmission index (ITI) and the output transmission index (OTI), which represent the power transmission efficiency from the actuated joints to the limbs and from the limbs to the moving platform, respectively. Considering the input transmission performance and output transmission performance

https://doi.org/10.1017/S0263574718001054 Published online by Cambridge University Press

simultaneously, the LTI can be defined as

$$\lambda_i = \frac{\left|\$_{\mathrm{A}i} \circ \$_{\mathrm{T}i}\right|}{\left|\$_{\mathrm{A}i} \circ \$_{\mathrm{T}i}\right|_{\max}}, \tag{18a}$$

$$\eta_i = \frac{\left|\$_{\mathrm{O}i} \circ \$_{\mathrm{T}i}\right|}{\left|\$_{\mathrm{O}i} \circ \$_{\mathrm{T}i}\right|_{\max}}, \tag{18b}$$

and

$$\Gamma = \min\left\{\lambda_i, \eta_i\right\}, \tag{18c}$$

where λ_i, η_i, and Γ denote the ITI, OTI, and LTI of limb i, respectively. $\$_{\mathrm{A}i}$ denotes the unit input twist screw (ITS) associated with the actuated joint in the limb i. $\$_{\mathrm{O}i}$ denotes the output twist screw (OTS) of the moving platform when all the actuators except that in the limb i are locked. $\$_{\mathrm{T}i}$ denotes the transmission wrench screw (TWS) of the limb i. The Γ ranges from zero to unity, and a larger Γ means better motion/force transmissibility. Although the twist/wrench screw in Eq. (18) contains combined units, these indices are dimensionless scalars. More details about Eq. (18) can be found in Ref. [38].

Equation (18c) cannot be applied directly to redundantly actuated PMs. Here, a recently proposed procedure[28] is used to evaluate the motion/force transmissibility of Hex4 PM by virtually separating the proposed PM into several one-DOF PMs that are actuated using two or more actuators. The validity of this method has been demonstrated in Ref. [28]. The procedure for evaluating the LTI of each point in the workspace is described below.

Step 1: Determine the TWS in each limb of the Hex4 PM. Without loss of generality, limb 1 is taken as an example. Via screw theory, the twist system is given as

$$\begin{cases} \$_{11} = \begin{pmatrix} 0 & 0 & 0; & 1 & 0 & 0 \end{pmatrix} \\ \$_{12} = \begin{pmatrix} 1 & 0 & 0; & 0 & 0 & 0 \end{pmatrix} \\ \$_{13} = \begin{pmatrix} 0 & \mathrm{c}_\alpha & -\mathrm{s}_\alpha; & 0 & q_1\mathrm{s}_\alpha & q_1\mathrm{c}_\alpha \end{pmatrix} \\ \$_{14} = \begin{pmatrix} 0 & \mathrm{c}_\alpha & -\mathrm{s}_\alpha; & -z_{B_1}\mathrm{c}_\alpha - y_{B_1}\mathrm{s}_\alpha & x_{B_1}\mathrm{s}_\alpha & x_{B_1}\mathrm{c}_\alpha \end{pmatrix} \end{cases}, \tag{19}$$

where $\$_{ij}$ represents the unit twist associated with the jth kinematic joint of the ith limb, and x_{B_i}, y_{B_i}, and z_{B_i} are the coordinates of points B_i with respect to the *O-XYZ*. The TWS should be linearly independent of all the passive twist screws. Since the actuated joint of limb 1 is a P joint, the TWS of limb 1 is reciprocal of [$\$_{12}$ $\$_{13}$ $\$_{14}$] and is given by

$$\$_{\mathrm{T1}} = \begin{pmatrix} x_{B_1} - q_1 & y_{B_1} & z_{B_1}; & 0 & -q_1 z_{B_1} & q_1 y_{B_1} \end{pmatrix}. \tag{20}$$

Similarly, the TWSs of the other three limbs can be derived as follows:

$$\begin{cases} \$_{\mathrm{T2}} = \begin{pmatrix} q_2 + x_{B_2} & y_{B_2} & z_{B_2}; & 0 & q_2 z_{B_2} & -q_2 y_{B_2} \end{pmatrix} \\ \$_{\mathrm{T3}} = \begin{pmatrix} 0 & e_3 & f_3; & -l_3 f_3 & 0 & 0 \end{pmatrix} \\ \$_{\mathrm{T4}} = \begin{pmatrix} 0 & -e_4 & f_4; & l_3 f_4 & 0 & 0 \end{pmatrix} \end{cases}. \tag{21}$$

Step 2: List the locked/active TWSs and form a new wrench system corresponding to a 2-PUR/2-RPU PM, from which the OTS is obtained. Locking the actuators installed in two arbitrary limbs, the corresponding TWSs in these two limbs turn into extra constraint wrenches of the moving platform. Adding the three original constraint wrenches, the moving platform sustains a five-order wrench system. The OTS can thus be obtained by reciprocal screw theory. For the Hex4 PM, there are $N = C_4^2 = 6$ combinations for selecting the two locked limbs. The corresponding locked/active combinations of limbs are listed in Table II.

https://doi.org/10.1017/S0263574718001054 Published online by Cambridge University Press

Table II. Locked/active combinations of limbs.

Case	Locked limbs	Active limbs	Wrench system of moving platform
1	1,2	3,4	$\boldsymbol{U}^1 = [\$_{C1}\ \$_{C2}\ \$_{C3}\ \$_{T1}\ \$_{T2}]$
2	1,3	2,4	$\boldsymbol{U}^2 = [\$_{C1}\ \$_{C2}\ \$_{C3}\ \$_{T1}\ \$_{T3}]$
3	1,4	2,3	$\boldsymbol{U}^3 = [\$_{C1}\ \$_{C2}\ \$_{C3}\ \$_{T1}\ \$_{T4}]$
4	2,3	1,4	$\boldsymbol{U}^4 = [\$_{C1}\ \$_{C2}\ \$_{C3}\ \$_{T2}\ \$_{T3}]$
5	2,4	1,3	$\boldsymbol{U}^5 = [\$_{C1}\ \$_{C2}\ \$_{C3}\ \$_{T2}\ \$_{T4}]$
6	3,4	1,2	$\boldsymbol{U}^6 = [\$_{C1}\ \$_{C2}\ \$_{C3}\ \$_{T3}\ \$_{T4}]$

The PM with case 1 is selected here as an example. As listed in Table II, the new wrench system imposed on the moving platform after locking two actuators can be written as

$$\boldsymbol{U}^1 = \left[\$_{C1}\ \$_{C2}\ \$_{C3}\ \$_{T1}\ \$_{T2}\right], \tag{22}$$

where $\$_{Ci}$ denote the ith unit constraint wrench imposed on the moving platform. Using reciprocal screw theory, the instantaneous one-DOF twist $\$_{\mathrm{O}}^1$ of the moving platform can be obtained from

$$\$_O^1 \circ \boldsymbol{U}^1 = 0. \tag{23}$$

There are six cases for the Hex4 PM. Once these cases are finished, proceed to Step 3. Until then, return to Step 2 and select the next case.

Step 3: Calculate the OTI and ITI. For a given output twist, the output transmissibility is influenced only by the TWSs of the active limbs. Thus, the OTI of case 1, which reflects the power coefficient between the active transmission wrenches and the output twist, can be written as

$$\eta^1 = \min\left\{ \frac{\left|\$_{\mathrm{O}}^1 \circ \$_{T3}\right| + \left|\$_{\mathrm{O}}^1 \circ \$_{T4}\right|}{\left|\$_{\mathrm{O}}^1 \circ \$_{T3}\right|_{\max} + \left|\$_{\mathrm{O}}^1 \circ \$_{T4}\right|}, \frac{\left|\$_{\mathrm{O}}^1 \circ \$_{T3}\right| + \left|\$_{\mathrm{O}}^1 \circ \$_{T4}\right|}{\left|\$_{\mathrm{O}}^1 \circ \$_{T3}\right| + \left|\$_{\mathrm{O}}^1 \circ \$_{T4}\right|_{\max}} \right\}. \tag{24}$$

From Eq. (24), the output transmissibility of the one-DOF PM is the coupled effect of two active limbs. For a redundantly actuated PM, the output transmission performance will exceed neither the maximum nor the minimum of those of the one-DOF PMs. Thus, the OTI of the redundantly actuated Hex4 PM in this study is defined as the average value of all cases as

$$\mathrm{OTI}: \eta = \frac{1}{6}\sum_{g=1}^{6} \eta^g. \tag{25}$$

In addition, the ITI of limb i (i =1, 2, 3, 4) can be easily obtained using Eq. (18a).

Step 4: Obtain the LTI of a certain configuration. Considering both the input and output transmissibility, the LTI for the Hex4 PM can be defined as

$$\mathrm{LTI}: \Gamma = \min\left\{\lambda_i, \eta\right\}. \tag{26}$$

For the Hex4 PM, the design parameters are set as follows: $l_1 = 250$ mm, $l_2 = 250$ mm, $l_3 = 400$ mm, $-40^\circ \le \alpha \le 40^\circ$, and $-40^\circ \le \beta \le 40^\circ$. Here, we consider the LTI distribution in a constant operation distance, $z_o = 600$ mm. The length of link parameter l is defined as

$$l = z_o + l_1 \mathrm{s}_{\beta_{\max}}, \tag{27}$$

https://doi.org/10.1017/S0263574718001054 Published online by Cambridge University Press

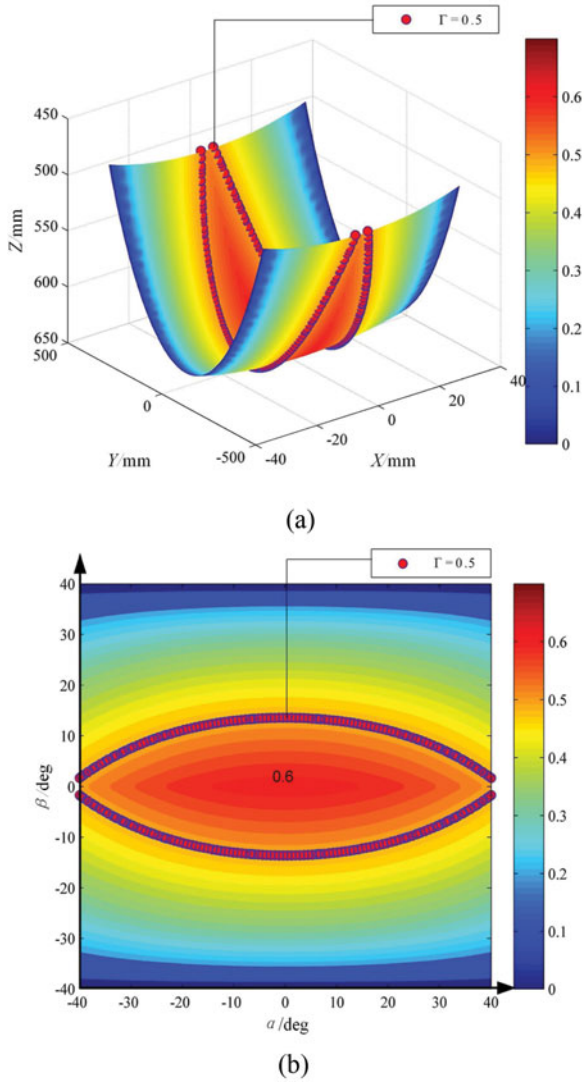

Fig. 4. LTI distributions of the Hex4 PM: (a) three-dimensional workspace and (b) orientation workspace.

which means that the Hex4 PM can achieve the extreme rotation of angle β in a given operation distance.

The LTI distributions of the Hex4 PM are shown in Fig. 4 where the color bar is used to represent the value of the LTI. The red points marked "$\Gamma = 0.5$" form two curves, and the LTI of each configuration on these curves is equal to 0.5. Figure 4(a) shows the LTI variation in a three-dimensional workspace with a tool-head length $H = 50$ mm. It is clear that the distribution is symmetrical about the planes $X = 0$ and $Y = 0$. In the orientation workspace as shown in Fig. 4(b), the LTI distribution is completely symmetrical with respect to both angles. Figure 4 shows that the closer the configuration is to the initial situation, the better the motion/force transmission performance will be. Furthermore, in contrast with angle α, the motion/force transmission performance decreases more quickly when angle β deviates from 0°.

The LTI distributions for different architectural parameters in the orientation workspace are shown in Fig. 5. It is obvious that no matter the variation of the design parameters (l_1, l_2, l_3), the tendency of the LTI in the orientation workspace is similar to the case for Fig. 4(b). Unlike the influences of design parameters l_1 and l_3, the tendencies of the LTI distributions shown in Fig. 5(d)–(f) are the same; the parameter l_2 has no impact on the LTI distribution, which may be related to the special structure of the PUR limb.

https://doi.org/10.1017/S0263574718001054 Published online by Cambridge University Press

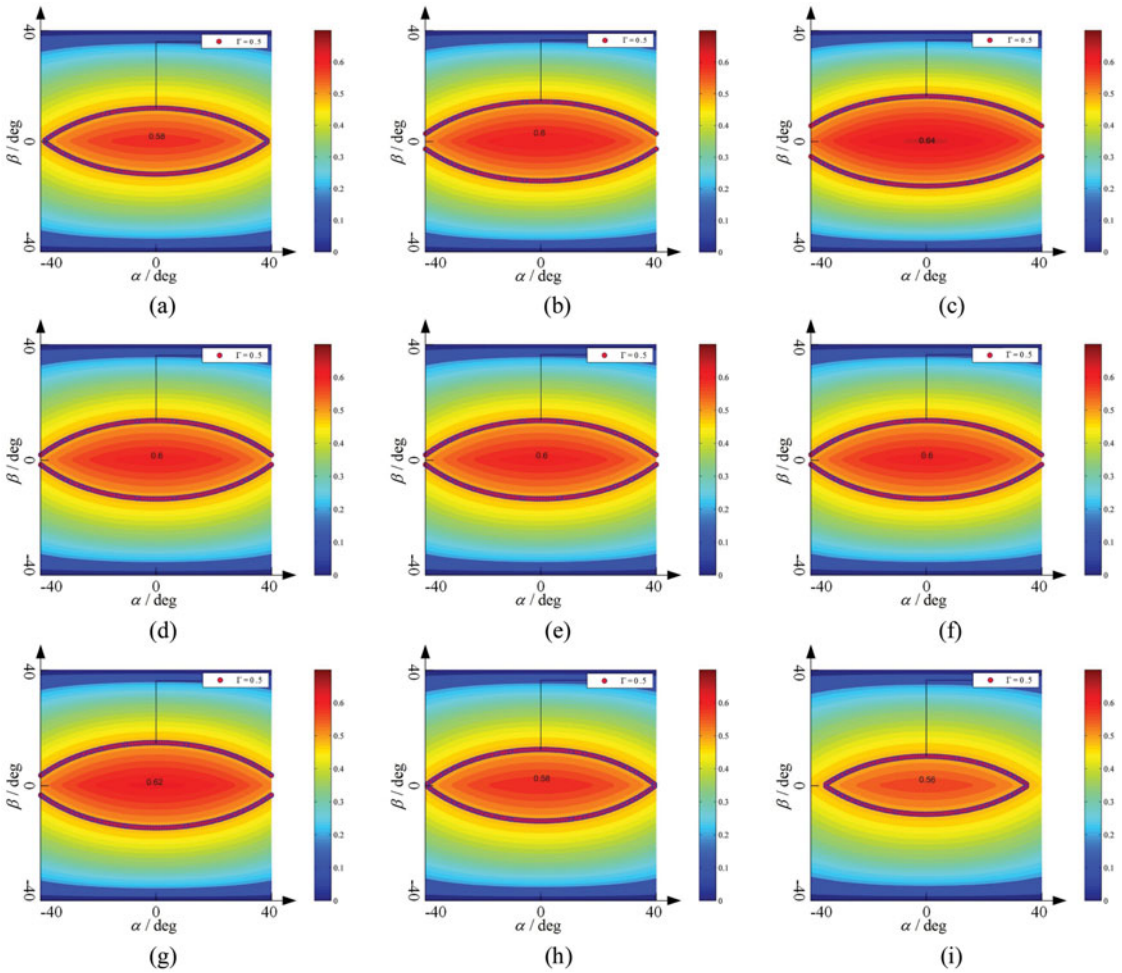

Fig. 5. LTI distributions for different architectural parameters: (a) $l_1 = 230$ mm, (b) $l_1 = 260$ mm, (c) $l_1 = 290$ mm, (d) $l_2 = 240$ mm, (e) $l_2 = 270$ mm, (f) $l_2 = 300$ mm, (g) $l_3 = 375$ mm, (h) $l_3 = 425$ mm, and (i) $l_3 = 475$ mm.

6.2. Global transmission index for redundantly actuated PMs

Because the LTI represents only the motion/force transmissibility in a single configuration, it is necessary to define an index that can describe the performance in a set of poses. According to the actual situation and the definition of the transmission angle,[43] it is assumed here that the region for which $\Gamma \geq 0.5$ can be considered as the GTW. The new index can thus measure the global motion/force transmissibility of a PM, and is defined as

$$\sigma = \frac{\int_{S_G} dW}{\int_S dW}, \tag{28}$$

where W is the reachable workspace, and S_G and S denote the areas of the GTW and overall possible workspace, respectively. Obviously, σ is dimensionless, and it ranges from zero to unity; the closer σ is to unity, the better the transmissibility of the Hex4 PM.

The effects of the architectural parameters l_1, l_2, and l_3 on the GTW are shown in Fig. 6. Figure 6(a) shows the relationship between the GTW parameter and l_1: the bigger the value of l_1, the better the σ value of the PM. Interestingly, Fig. 6(b) shows that no matter how l_2 changes, the value of σ remains the same. Figure 6(c) shows the relationship between the GTW parameter and l_3: the bigger the value of l_3, the worse the σ value of the Hex4 PM. Consequently, the influences of architectural parameters are different with each other, which should be considered in the dimensional optimization.

https://doi.org/10.1017/S0263574718001054 Published online by Cambridge University Press

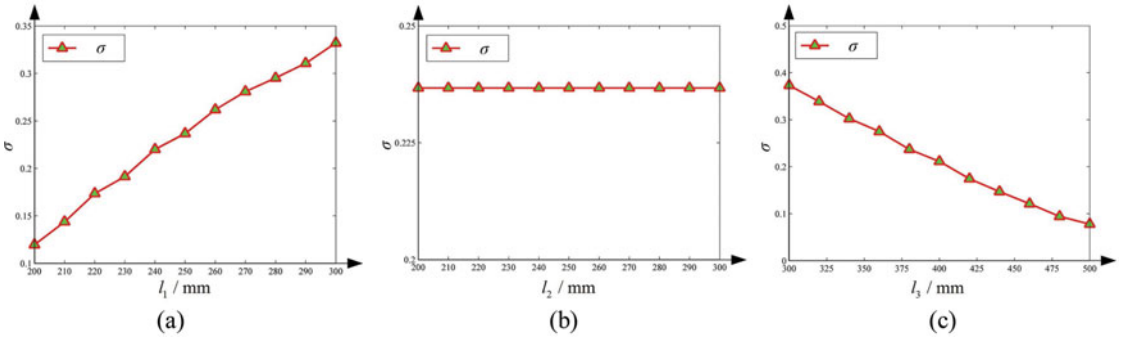

Fig. 6. Tendencies of σ for different architectural parameters: (a) l_1, (b) l_2, and (c) l_3.

7. Singularity Analysis

Kinematic analysis and optimization of a PM inevitably requires a singularity analysis. Singular configurations can cause a PM to be uncontrollable or have undesirable stiffness, both of which should be avoided before planning the motion trajectory. Gosselin and Angeles[44] obtained kinematic singularities from the mathematical characteristics of Jacobian matrices, whereas Liu *et al.*[45] did so by means of motion/force transmissibility. Here, singularities of the Hex4 PM are investigated using the classification proposed in ref. [45].

7.1. Input transmission singularity and inverse kinematic singularity

An input transmission singularity occurs when the *i*th limb cannot obtain power from the corresponding actuator,[45] i.e., the transmission efficiency between the ITS and TWS is zero:

$$\$_{\mathrm{A}i} \circ \$_{\mathrm{T}i} = 0. \tag{29}$$

Equation (29) holds only when rotational angle α or β is at an extreme value. For cases of extreme β (either positive or negative) as shown in Fig. 7(a), the green points marked "input transmission singularity" form two curves of input transmission singular loci, and each configuration on these curves is singular because limb 1 or 2 is perpendicular to the guide A_1A_2. For cases of extreme α, as shown in Fig. 8, the center of the U joint of limb 3 or 4 overlaps that of the R joint, which cannot happen in a real application.

In fact, an input transmission singularity is the same as an inverse kinematic singularity.[44] A point on the curve of input transmission singular loci also corresponds to a configuration in which the PM has an inverse kinematic singularity, i.e., $|\boldsymbol{J}_x^{\mathrm{T}}\boldsymbol{J}_x| \neq 0$ and $|\boldsymbol{J}_q| = 0$, in which any one of $J_{q_{ii}}$ ($i = 1, 2, 3, 4$) is equal to zero.

(1) $J_{q_{11}} = 0$ or $J_{q_{22}} = 0$ holds if

$$l = \left| z_o \mp l_1 \mathrm{s}_\beta \right|. \tag{30}$$

The above condition occurs only if link A_iB_i ($i = 1, 2$) is perpendicular to slider A_1A_2. Two singular configurations corresponding to Eq. (30) are shown in Fig. 7(a). Additionally, if links A_1B_1 and A_2B_2 are both perpendicular to the slider, the Hex 4 PM is also at an inverse kinematic singular configuration, as shown in Fig. 7(b).

Here, screw theory is used to verify the situation when link A_1B_1 is perpendicular to slider A_1A_2. The twist system of limb 1 can be written as

$$\begin{cases} \$_{11} = \begin{pmatrix} 0 & 0 & 0; & 1 & 0 & 0 \end{pmatrix} \\ \$_{12} = \begin{pmatrix} 1 & 0 & 0; & 0 & 0 & 0 \end{pmatrix} \\ \$_{13} = \begin{pmatrix} 0 & \mathrm{c}_\alpha & -\mathrm{s}_\alpha; & 0 & q_1\mathrm{s}_\alpha & q_1\mathrm{c}_\alpha \end{pmatrix} \\ \$_{14} = \begin{pmatrix} 0 & \mathrm{c}_\alpha & -\mathrm{s}_\alpha; & -z_{B_1}\mathrm{c}_\alpha - y_{B_1}\mathrm{s}_\alpha & q_1\mathrm{s}_\alpha & q_1\mathrm{c}_\alpha \end{pmatrix} \end{cases}. \tag{31}$$

https://doi.org/10.1017/S0263574718001054 Published online by Cambridge University Press

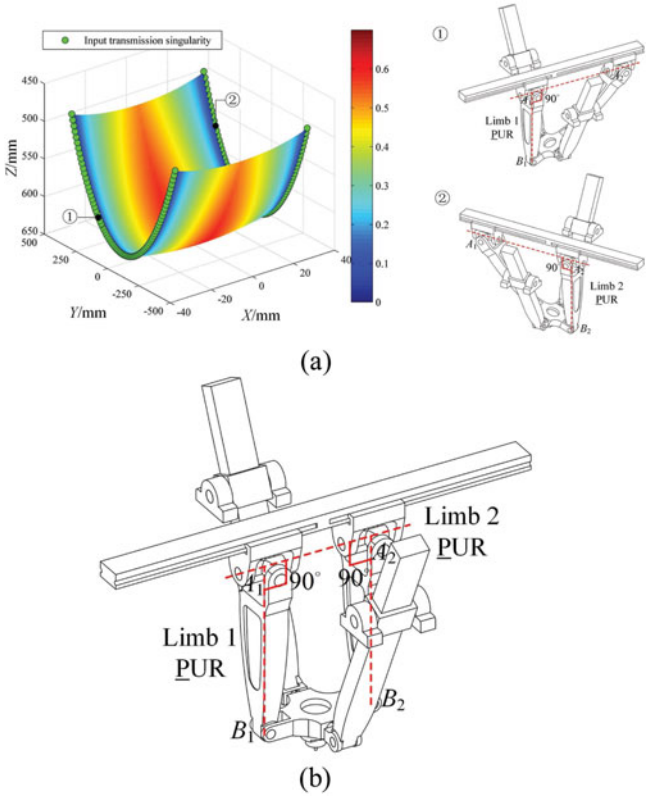

Fig. 7. Input transmission singularities when β is at an extreme value: (a) first configuration and (b) second configuration.

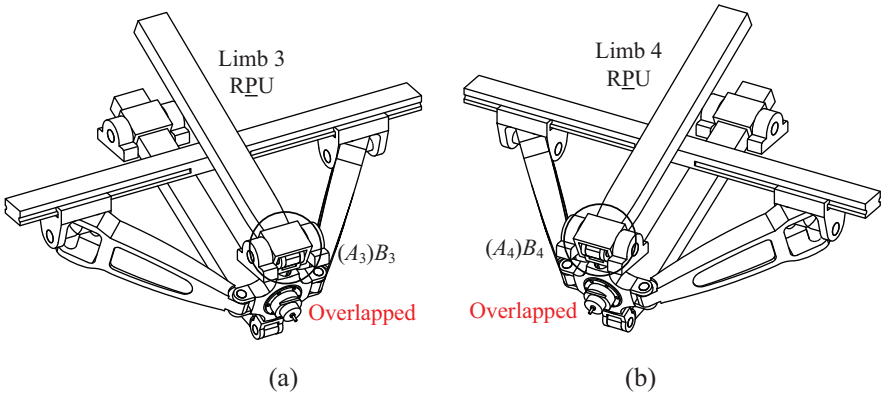

Fig. 8. Input transmission singularities when α is at an extreme value: (a) first configuration and (b) second configuration.

From Eq. (31), we find that $\$_{14}$ is a combination of $\$_{11}$ and $\$_{13}$, so the rank of the twist system is three. The wrench system of limb 1 can be expressed as

$$\begin{cases} \$_{11}^r = \begin{pmatrix} 0 & 0 & 0; & 0 & s_\alpha & c_\alpha \end{pmatrix} \\ \$_{12}^r = \begin{pmatrix} 0 & 1 & 0; & 0 & -q_1 \tan_\alpha & 0 \end{pmatrix} \\ \$_{13}^r = \begin{pmatrix} 0 & 0 & 1; & 0 & -q_1 & 0 \end{pmatrix} \end{cases}, \tag{32}$$

where $\$_{ij}^r$ denotes the jth unit constraint wrench exerted on the moving platform by the ith limb. Similarly, the wrench systems of the other three limbs can be derived as

https://doi.org/10.1017/S0263574718001054 Published online by Cambridge University Press

follows:

$$\begin{cases} \$_{21}^{r} = \begin{pmatrix} 0 & 0 & 0; & 0 & \mathrm{s}_\alpha & \mathrm{c}_\alpha \end{pmatrix} \\ \$_{22}^{r} = \begin{pmatrix} 0 & -\mathrm{c}_\alpha & \mathrm{s}_\alpha; & 0 & 0 & 0 \end{pmatrix} \end{cases}, \tag{33a}$$

$$\begin{cases} \$_{31}^{r} = \begin{pmatrix} 0 & 0 & 0; & 0 & \mathrm{s}_\alpha & \mathrm{c}_\alpha \end{pmatrix} \\ \$_{32}^{r} = \begin{pmatrix} 1 & 0 & 0; & 0 & z_o/\mathrm{c}_\alpha & 0 \end{pmatrix} \end{cases}, \tag{33b}$$

and

$$\begin{cases} \$_{41}^{r} = \begin{pmatrix} 0 & 0 & 0; & 0 & \mathrm{s}_\alpha & \mathrm{c}_\alpha \end{pmatrix} \\ \$_{42}^{r} = \begin{pmatrix} 1 & 0 & 0; & 0 & z_o/\mathrm{c}_\alpha & 0 \end{pmatrix} \end{cases}. \tag{33c}$$

Therefore, the twist system that is simultaneously reciprocal to Eqs. (32) and (33) can be written as

$$\begin{cases} \$_{1}^{pm} = \begin{pmatrix} 1 & 0 & 0; & 0 & 0 & 0 \end{pmatrix} \\ \$_{2}^{pm} = \begin{pmatrix} 0 & \mathrm{c}_\alpha & -\mathrm{s}_\alpha; & -z_o & q_1\mathrm{s}_\alpha & q_1\mathrm{c}_\alpha \end{pmatrix} \end{cases}. \tag{34}$$

Equation (34) shows that the Hex4 PM only remains two DOFs in this configuration: one rotation around the X-axis and another around the y-axis.

For the case of Fig. 7(b), the wrench system of limb 2 is different from that of Eq. (33a), being given by

$$\begin{cases} \$_{21}^{r} = \begin{pmatrix} 0 & 0 & 0; & 0 & \mathrm{s}_\alpha & \mathrm{c}_\alpha \end{pmatrix} \\ \$_{22}^{r} = \begin{pmatrix} 0 & 1 & 0; & 0 & q_1\mathrm{tan}_\alpha & 0 \end{pmatrix} \\ \$_{23}^{r} = \begin{pmatrix} 0 & 0 & 1; & 0 & q_1 & 0 \end{pmatrix} \end{cases}. \tag{35}$$

where tan denotes the tangent function.

The twist system in this singular configuration can be written as

$$\$_{1}^{pm} = \begin{pmatrix} 1 & 0 & 0; & 0 & 0 & 0 \end{pmatrix}. \tag{36}$$

Equation (36) shows that in this configuration, the only DOF of the Hex4 PM is rotation around the X-axis.

(2) $J_{q_{33}} = 0$ or $J_{q_{44}} = 0$ holds if

$$\begin{cases} \alpha = \mp\arccos\left(\dfrac{l_2}{l_3}\right) \\ z_o = \dfrac{l_2\sqrt{{l_3}^2 - {l_2}^2}}{l_3 c_\alpha} \end{cases}. \tag{37}$$

We find that the angle β has no impact on the inverse singularities. The configurations expressed by Eq. (37) correspond to those shown in Fig. 8; however, these cannot occur in a real application.

7.2. Output transmission singularity

An output transmission singularity of a PM with actuation redundancy occurs only if the motion of the moving platform cannot be achieved by the TWSs, i.e., the mean instantaneous output power produced by the TWS and OTS of the subsidiary one-DOF PMs is zero:

$$\eta = 0. \tag{38}$$

However, based on Eqs. (24) and (25), the output transmission efficiency of the PM cannot be zero. In other words, there is no configuration in which the output power of each of the one-DOF PMs is zero. Consequently, the Hex4 PM has no output transmission singularity.

https://doi.org/10.1017/S0263574718001054 Published online by Cambridge University Press

7.3. Combined transmission singularity

A combined transmission singularity occurs only if ITI = 0 and OTI = 0 simultaneously. Combining the above analyses, it is clear that the Hex4 PM has no combined transmission singularity.

In summarizing the above analyses, the Hex4 PM only has inverse transmission singularities, which can be avoided in actual applications.

8. Optimization of Design Parameters

In this study, optimization of the design parameters of the Hex4 PM is based on the GTW. The rotation angles and operating distance are set as follows: $\alpha \in [-40^\circ, 40^\circ]$, $\beta \in [-40^\circ, 40^\circ]$, and $z_o = 1.5l_3$. Under actual conditions, the design parameters of the mechanism cannot be selected arbitrarily because of the effects of assembly and movement. There are many methods to optimize the design parameters, such as genetic algorithm[46] and interval analysis,[47,48] which can consider many different constraints simultaneously, and provide guaranteed results. Here, the parameter-finiteness normalization method (PFNM) proposed by Liu. *et al*.[49] is used to optimize the design parameters of Hex4 PM. Compared to other methods, the PFNM achieves the reduction of the parameter number and converts the infinite parameter space into a finite space. Meanwhile, based on the normalized factor, this method limits the boundary of each normalized parameter. Through this method, the performance distributions of the objective mechanism with different design parameters can be found in the finite design space. For Hex4 PM, the design parameters are normalized as

$$\begin{cases} D = \dfrac{l_1 + l_2 + l_3}{3} \\ r_1 = \dfrac{l_1}{D}, r_2 = \dfrac{l_2}{D}, r_3 = \dfrac{l_3}{D} \end{cases}, \tag{39}$$

where D is a normalized factor and r_i is a normalized non-dimensional parameter. Considering practical applications, the normalized parameters should satisfy

$$\begin{cases} r_1, r_2 \le r_3 \\ 0 < r_1, r_2, r_3 < 3 \end{cases}. \tag{40}$$

As shown in Fig. 9, the parameter design space[49] includes all possible points. The relationship between the parameters in three-dimensional space (r_1, r_2, r_3) and those in plan space (s, t) is described as follows:

$$\begin{cases} r_1 = \dfrac{3}{2} + \dfrac{\sqrt{3}}{2}t - \dfrac{s}{2} \\ r_2 = \dfrac{3}{2} - \dfrac{\sqrt{3}}{2}t - \dfrac{s}{2} \\ r_3 = s \end{cases} \quad \text{or} \quad \begin{cases} s = r_3 \\ t = \dfrac{r_1 - r_2}{\sqrt{3}} \end{cases}. \tag{41}$$

The design steps for performance optimization are as follows.

Step 1: Identify the regions. The distributions of GTW can be obtained as shown in Fig. 10, which has been divided into three regions with different colors based on the range of σ. Region I—in which $\sigma \in (0, 0.2)$—is regarded as having poor global motion/force transmission, region II—in which $\sigma \in [0.2, 0.4)$—is regarded as having medium global motion/force transmission, and region III—in which $\sigma \ge 0.4$—is regarded as having good global motion/force transmission.

Step 2: Select three groups of data points randomly from each region I, II, and III; altogether, nine groups of data points are chosen in this study. For each group, the non-dimensional parameters

https://doi.org/10.1017/S0263574718001054 Published online by Cambridge University Press

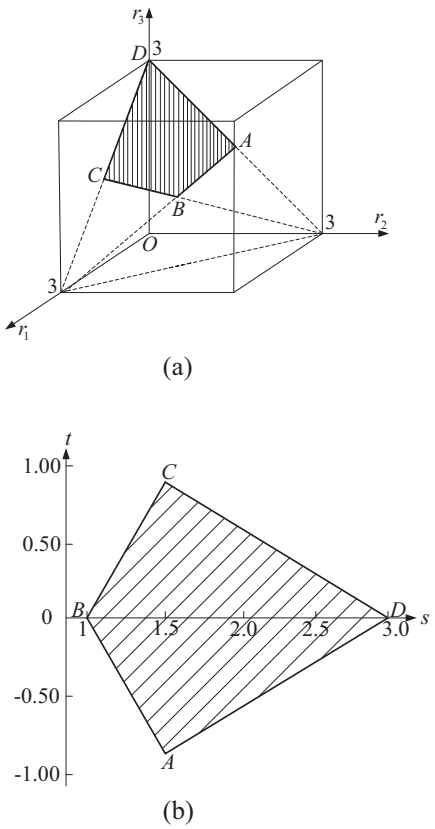

Fig. 9. Model of the parameter design space: (a) spatial view and (b) plan view.

r_1, r_2, and r_3 can be obtained using Eq. (41). Using Eqs. (39) and (41), one can then obtain the design parameters l_1, l_2, and l_3 and the two plan-space parameters s and t, as listed in Table III.

Step 3: Determine the normalized factor D and dimensional parameters l_1, l_2, and l_3. In view of the actual operating region, the normalized factor D is determined as 500 mm. For example, the design parameters in group 1 are chosen as the results, i.e., $r_1 = 0.95$, $r_2 = 0.37$, and $r_3 = 1.68$. The values of l_i can then be obtained using Eq. (39), i.e., $l_1 = 475$ mm, $l_2 = 185$ mm, and $l_3 = 840$ mm.

Step 4: Check whether the dimensional parameters obtained in Step 3 are suitable for actual applications. If the actual assembly conditions are satisfied, the procedure is finished; otherwise, return to Step 3, choose another group of data from the region, and repeat Steps 3 and 4.

Figure 11 shows comparisons of the motion/force transmissibility in regions I, II, and III, for which the design parameters in groups 3, 6, and 9 are chosen as examples. As shown in Fig. 11(c), the value of GTW in region III is 0.437, which is better than that in either of the other two examples. The results demonstrate that region III could be selected as the optimal region, and the parameters in group 9 can be chosen as optimized design parameters.

9. Conclusions

A new 2R1T overconstrained PM with actuation redundancy, Hex4 PM, is proposed. This PM is actuated by four P joints, and two of them are mounted on the fixed base to reduce the movable mass and improve the dynamic response. Mobility analysis indicates that the proposed PKM has one translational DOF and two rotational DOFs. The inverse kinematics are straightforward and consequently can simplify the dynamic modeling and control. The LTI and GTW are used to evaluate

https://doi.org/10.1017/S0263574718001054 Published online by Cambridge University Press

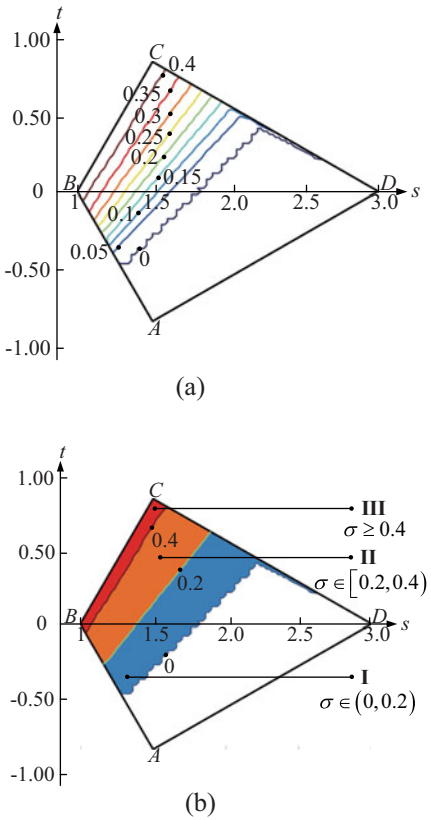

Fig. 10. Optimization of GTW for the Hex4 PM: (a) distribution of σ and (b) design regions I, II, and III.

Table III. GTW in the design regions.

Region	Group	s	t	r_1	r_2	r_3	l_1	l_2	l_3	GTW
	1	1.68	0.34	0.95	0.37	1.68	475	185	840	0.189
I	2	1.72	0.26	0.87	0.41	1.72	435	205	860	0.124
	3	1.76	0.18	0.78	0.46	1.76	390	230	880	0.063
	4	1.40	0.46	1.20	0.40	1.40	600	200	700	0.387
II	5	1.56	0.50	1.15	0.29	1.56	575	145	780	0.322
	6	1.58	0.36	1.02	0.4	1.58	510	200	790	0.258
	7	1.24	0.30	1.14	0.62	1.24	570	310	620	0.414
III	8	1.26	0.36	1.18	0.56	1.26	590	280	630	0.422
	9	1.30	0.48	1.27	0.43	1.3	635	215	650	0.437

the motion/force transmission characteristics of the Hex4 PM. The variation tendencies of the two indices show that the influence of each link parameter (l_1, l_2, and l_3) is totally different. Based on the motion/force transmissibility, it is found that the proposed PM only has inverse transmission singularities, which can be avoided in actual applications. An optimized Hex4 PM was obtained after optimizing the link parameters with respect to the GTW.

From this paper, it can be concluded that the Hex4 PM has a great potential in applications where high rigidity, dexterity and accuracy are required. And the LTI can be widely used for performance research works focusing on mechanisms with actuation redundancy. Future work includes building a prototype of the Hex4 PM based on the optimal parameters, and conducting some experiments such as calibration and verification.

https://doi.org/10.1017/S0263574718001054 Published online by Cambridge University Press

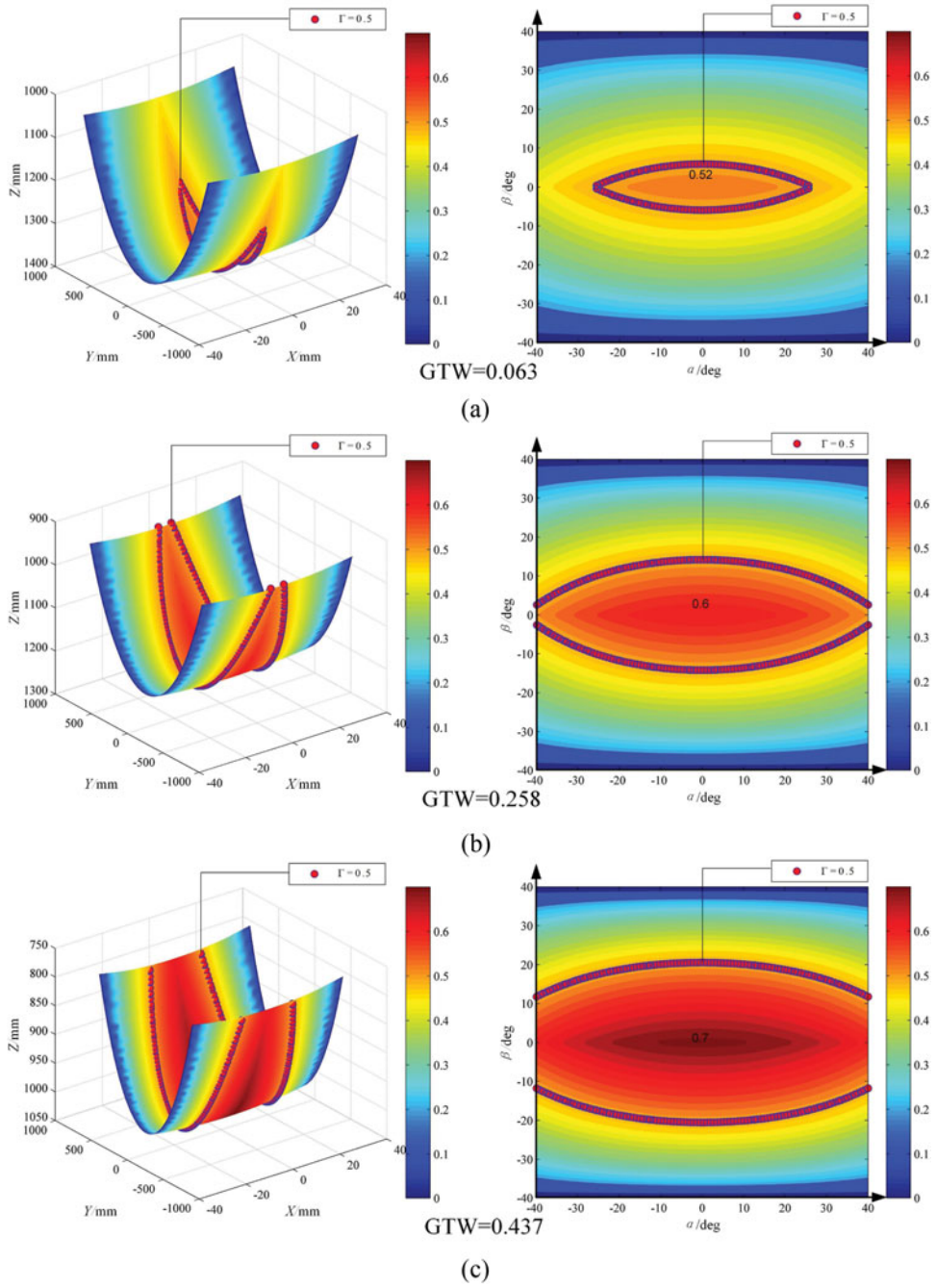

Fig. 11. Comparisons of motion/force transmissibility: (a) region I with $l_1 = 390$ mm, $l_2 = 230$ mm, and $l_3 = 880$ mm (group 3), (b) region II with $l_1 = 510$ mm, $l_2 = 200$ mm, and $l_3 = 790$ mm (group 6), and (c) region III with $l_1 = 635$ mm, $l_2 = 215$ mm, and $l_3 = 650$ mm (group 9).

Acknowledgements

This work was supported by National Natural Science Foundation of China (Grant No. 51525504, 51475431, and U1713202).

References

1. K. H. Hunt, "Structural kinematics of in-parallel-actuated robot-arms," *ASME J. Mech. Robot.* **105**(4), 705–712 (1983).
2. J. Wahl, "Articulated tool head," WIPO Patent No. WO/2000/025976 (2000).

https://doi.org/10.1017/S0263574718001054 Published online by Cambridge University Press

3. Z. M. Bi and Y. Jin, "Kinematic modeling of Exechon parallel kinematic machine," *Robot. Comput. Integr. Manuf.* **27**(1), 186–193 (2011).
4. B. Siciliano, "The Tricept robot: Inverse kinematics, manipulability analysis and closed-loop direct kinematics algorithm," *Robotica* **17**(17), 437–445 (1999).
5. Q. C. Li and J. M. Hervé, "Type synthesis of 3-DOF RPR-equivalent parallel mechanisms," *IEEE Trans. Robot.* **30**(6), 1333–1343 (2014).
6. R. S. Stoughton and T. Arai, "A modified stewart platform manipulator with improved dexterity," *IEEE Trans. Robot. Autom.* **9**(2), 166–173 (1993).
7. R. Clavel, "A Fast Robot with Parallel Geometry," Proceedings of the 18th International Symposium on Industrial Robots, Lausanne, Switzerland (1988) pp. 91–100.
8. J. P. Merlet, "Redundant parallel manipulators," *Lab. Rob. Autom.* **8**(1), 17–24 (1996).
9. S. Kim, "Operational Quality Analysis of Parallel Manipulators with Actuation Redundancy," *Proceedings of the IEEE International Conference on Robotics and Automation*, Albuquerque, New Mexico (Apr. 1997) pp. 2651–2656.
10. J. S. Wang, J. Wu, T. M. Li and X. J. Liu, "Workspace and singularity analysis of a 3-DOF planar parallel manipulator with actuation redundancy," *Robotica* **27**(1), 51–57 (2009).
11. J. A. Saglia, J. S. Dai and D. G. Caldwell, "Geometry and kinematic analysis of a redundantly actuated parallel mechanism that eliminates singularities and improves dexterity," *ASME J. Mech. Robot.* **130**(12), 124501 (2008).
12. S. H. Kim, D. Jeon, H. P. Shin, W. In and J. Kim, "Design and analysis of decoupled parallel mechanism with redundant actuator," *I. J. Precis. Eng. Manuf.* **10**(4), 93–99 (2009).
13. C. Z. Wang, Y. F. Fang, S. Guo and Y. Q. Chen, "Design and kinematical performance analysis of a 3-RUS/RRR redundantly actuated parallel mechanism for ankle rehabilitation," *ASME J. Mech. Robot.* **5**(4), 1585–1606 (2013).
14. M. Gouttefarde and C. M. Gosselin, "Wrench-closure workspace of six-DOF parallel mechanism driven by 7 cables," *Trans. CSME/de la SCGM*, **29**(4), 541–552 (2005).
15. S. Bouchard, C. M. Gosselin and B. Moore, "On the ability of a cable-driven robot to generate a prescribed set of wrenches," *ASME J. Mech. Robot.* **2**(1), 47–58 (2010).
16. V. Garg, J. A. Carretero and S. B. Nokleby, "A new method to calculate the force and moment workspaces of actuation redundant spatial parallel manipulators," *ASME J. Mech. Robot.* **1**(1), 402–421 (2009).
17. J. F. Gardner, V. Kumar and J. H. Ho, "Kinematics and Control of Redundantly Actuated Closed Chains," *Proceedings of the IEEE International Conference on Robotics and Automation*, Scottsdale, AZ, USA, (1989) pp. 418–424.
18. V. Kumar and J. F. Gardner, "Kinematics of redundantly actuated closed kinematic chains," *IEEE Trans. Rob. Autom.* **6**(2), 269–274 (1999).
19. J. Kim, F. C. Park, S. J. Ryu, J. Kim, J. C. Hwang, C. Park and C. C. Iurascu, "Design and analysis of a redundantly actuated parallel mechanism for rapid machining," *IEEE Trans. Rob. Autom.* **17**(4), 423–434 (2001).
20. D. Zhang and J. Lei, "Kinematic analysis of a novel 3-DOF actuation redundant parallel manipulator using artificial intelligence approach," *Robot. Comput. Integr. Manuf.* **27**(1), 157–163 (2011).
21. D. Zhang, Z. Gao, X. P. Su and J. Li, "A comparison study of three degree-of-freedom parallel robotic machine tools with/without actuation redundancy," *Int. J. Comput. Integr. Manuf.* **25**(3), 230–247 (2012).
22. H. Shin, S. Lee, J. I. Jeong and J. Kim, "Antagonistic stiffness optimization of redundantly actuated parallel manipulators in a predefined workspace," *IEEE/ASME Trans. Mechatronics.* **18**(3), 1161–1169 (2013).
23. L. P. Wang, J. Wu, J. S. Wang and Z. You, "An experimental study of a redundantly actuated parallel manipulator for a 5-DOF hybrid machine tool," *IEEE/ASME Trans. Mechatronics.* **14**(1), 72–81 (2009).
24. J. Wu, J. S. Wang, L. P. Wang and T. M. Li, "Dexterity and stiffness analysis of a three-degree-of-freedom planar parallel manipulator with actuation redundancy," *Proc. Inst. Mech. Eng. Part C: J. Mech. Eng. Sci.* **221**(8), 961–969 (2007).
25. J. A. Saglia, N. G. Tsagarakis, J. S. Dai and D. G. Caldwell, "A high-performance redundantly actuated parallel mechanism for ankle rehabilitation," *Int. J. Rob. Res.* **28**(9), 1216–1227 (2009).
26. Y. Jin, X. W. Kong and C. Higgins, "Kinematic Design of a New Parallel Kinematic Machine for Aircraft Wing Assembly," *Proceedings of the 10th IEEE International Conference on Industrial Informatics*, Beijing, China (2012) pp. 669–674.
27. G. Kiper and B. Bağdadioğlu, "Function Generation Synthesis with a 2-DoF Overconstrained Double-Spherical 7R Mechanism Using the Method of Decomposition and Least Squares Approximation," **In:** *New Trends in Mechanism and Machine Science: From Fundamentals to Industrial Applications* (P. Flores and F. Viadero, eds.) (Springer International Publishing, Cham, 2015) **24**, pp. 175–183.
28. Q. C. Li, N. B. Zhang and F. B. Wang, "New indices for optimal design of redundantly actuated parallel manipulators," *ASME J. Mech. Robot* **9**(1), 011007 (2017).
29. L. M. Xu, Q. C. Li, N. B. Zhang and Q. H. Chen, "Mobility, kinematic analysis, and dimensional optimization of new three-degrees-of-freedom parallel manipulator with actuation redundancy," *ASME J. Mech. Robot* **9**(4), 041008 (2017).
30. Q. C. Li, L. M. Xu, Q. H. Chen and W. Ye, "New family of RPR-equivalent parallel mechanisms: Design and application," *Chin. J. Mech. Eng.* **30**(2), 217–221 (2017).
31. R. S. Stoughton and T. Arai, "A modified stewart platform manipulator with improved dexterity," *IEEE Trans. Rob. Autom.* **9**(2), 166–173 (1993).

32. J. Angeles and C. S. López-Cajún, "Kinematic isotropy and the conditioning index of serial robotic manipulators," *Int. J. Rob. Res.* **11**(6), 560–571 (1992).
33. J. P. Merlet, "Jacobian, manipulability, condition number, and accuracy of parallel robots," *ASME J. Mech. Robot* **128**(1), 199–206 (2006).
34. R. S. Ball, *A Treatise on the Theory of Screws* (Cambridge University Press, Cambridge, UK, 1900).
35. M. S. C. Yuan, F. Freudenstein and L. S. Woo, "Kinematic analysis of spatial mechanism by means of screw coordinates: Part 2-Analysis of spatial mechanisms," *J. Eng. Indus.* **91**(1), 67–73 (1971).
36. G. Sutherland and B. Roth, "A transmission index for spatial mechanisms," *J. Eng. Indu.* **95**(2), 589–597 (1973).
37. M. J. Tsai and H. W. Lee, "Generalized evaluation for the transmission performance of mechanisms," *Mech. Mach. Theory* **29**(4), 607–618 (1994).
38. J. S. Wang, C. Wu and X. J. Liu, "Performance evaluation of parallel manipulators: Motion/force transmissibility and its index," *Mech. Mach. Theory* **45**(10), 1462–1476 (2010).
39. F. G. Xie, X. J. Liu and Y. H. Zhou, "Optimization of a redundantly actuated parallel kinematic mechanism for a 5-degree-of-freedom hybrid machine tool," *Proc. Inst. Mech. Eng. Part B: J. Eng. Manuf.* **228**(12), 1630–1641 (2014).
40. F. G. Xie, X. J. Liu and Y. H. Zhou, "Development and experimental study of a redundant hybrid machine with five-face milling capability in one setup," *I. J. Precis. Eng. Man* **15**(1), 13–21 (2014).
41. Z. Huang and Q. C. Li, "Type synthesis of symmetrical lower-mobility parallel mechanisms using the constraint-synthesis method," *Int. J. Rob. Res.* **22**(1), 59–79 (2003).
42. J. M. Hervé, "Analyse structurelle des mécanismes par groupe des déplacements," *Mech. Mach. Theory* **13**(4), 437–450 (1978).
43. D. C. Tao, *Applied Linkage Synthesis* (Addison-Wesley Reading, MA, 1964).
44. C. M. Gosselin and J. Angeles, "Singularity analysis of closed-loop kinematic chains," *IEEE Trans. Rob. Autom.* **6**(3), 281–290 (1990).
45. X. J. Liu, C. Wu and J. S. Wang, "A new approach for singularity analysis and closeness measurement to singularities of parallel manipulators," *ASME J. Mech. Robot* **4**(4), 61–68 (2012).
46. R. Kelaiaia, O. Company and A. Zaatri, "Multiobjective optimization of parallel kinematic mechanisms by the genetic algorithms," *Robotica* **30**(5), 783–797 (2012).
47. R. E. Moore, *Methods and Applications of Interval Analysis* (Studies in Applied Mathematics, Philadelphia, PA, USA, 1979).
48. J. P. Merlet, "Interval Analysis and Robotics," *Proceedings of the 13th International Symposium on Robotics Research*, Hiroshima, Japan (Nov., 2007) pp. 147–156.
49. X. J. Liu and J. S. Wang, "A new methodology for optimal kinematic design of parallel mechanisms," *Mech. Mach. Theory* **42**(9), 1210–122 (2007).

https://doi.org/10.1017/S0263574718001054 Published online by Cambridge University Press